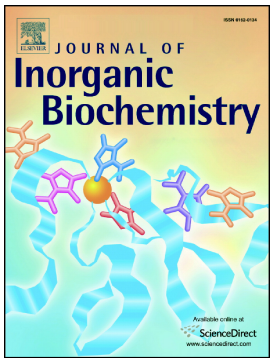

A lysosome-targeted ruthenium(II) polypyridyl complex as photodynamic anticancer agent

Jun Chen, Qin Tao, Jian Wu, Mengmeng Wang, Zhi Su, Yong Qian, Tao Yu, Yan Wang, Xuling Xue, Hong-Ke Liu

PII: S0162-0134(20)30160-4

DOI: https://doi.org/10.1016/j.jinorgbio.2020.111132

Reference: JIB 111132

To appear in: *Journal of Inorganic Biochemistry*

Received date: 6 March 2020

Revised date: 29 May 2020

Accepted date: 29 May 2020

Please cite this article as: J. Chen, Q. Tao, J. Wu, et al., A lysosome-targeted ruthenium(II) polypyridyl complex as photodynamic anticancer agent, *Journal of Inorganic Biochemistry* (2020), https://doi.org/10.1016/j.jinorgbio.2020.111132

A lysosome-targeted ruthenium(II) polypyridyl complex as photodynamic anticancer agent

Jun Chen [a,b], Qin Tao [b], Jian Wu [b], Mengmeng Wang [b], Zhi Su [b], Yong Qian [b], Tao Yu [c], Yan Wang [a,*], Xuling Xue [b,*] and Hong-Ke Liu [b,*]

[a] Anhui Key Laboratory of Functional Coordination Compounds, School of Chemistry and Chemical Engineering, Anqing Normal University, Anqing, 246011, China

[b] Jiangsu Collaborative Innovation Center of Biomedical Functional Materials, College of Chemistry and Materials Science, Nanjing Normal University, Nanjing, 210023, China

[c] Department of Chemistry, University of North Dakota, 151 Cornell St., Grand Forks, North Dakota, USA, 58202

[*]E-mail: njwangy@live.com; xuexuling87@163.com; liuhongke@njnu.edu.cn.

Abstract

Polypyridyl ruthenium complexes as novel photosensitizers had drawn attention due to its high selectivity towards cancer cells and low toxicity to normal cells. Herein, we synthesized a lysosome-targeted polypyridyl ruthenium complex **Rhein-Ru(bpy)$_3$** (bpy=2,2′-bipyridine, rhein=4,5-dihydroxy-9,10-dioxoanthracene-2-carboxylic acid), tethering with the Chinese medicine herb rhein. **Rhein-Ru(bpy)$_3$** exhibited high phototoxicity with short time of irradiation against tumor cell lines with the IC_{50} value of 2.4~8.7 μM, and higher cytotoxicity against cisplatin-resistant A2780 cell lines, suggesting that **Rhein-Ru(bpy)$_3$** could overcome the cisplatin resistance. Moreover, **Rhein-Ru(bpy)$_3$** displayed low cytotoxicity towards cell lines in dark incubation,

which was beneficial to reduce the toxic side effects towards normal cell lines. Besides, the confocal imaging and western blotting assay results suggested that **Rhein-Ru(bpy)$_3$** could induce cancer cell death through the autophagy pathway. These results inspired us that lysosome-targeted photosensitizers based on ruthenium complexes showed great potential for photodynamic therapy (PDT) application in cancer treatment.

1. Introduction

Photodynamic therapy (PDT) as a new candidate for cancer therapy has attracted great deal of attention and has been applied to clinical research due to its high selectivity, non-invasive property, low resistance and dark toxicity [1,2]. Generally, photosensitizer was activated by light irradiation and generated energy to transfer oxygen to reactive oxygen species (ROS) [3,4]. ROS was considered as a main toxic source to exert anticancer effect by destroying the cytoplasmic proteins and other biomolecules [5,6]. However, ROS has only a short lifetime of ~200 ns and a short diffusion range (~20 nm), which rendered it to act only in the immediate vicinity [7]. Therefore, the ROS generation should be extremely restricted to the important targets, like mitochondria, nucleus and lysosomes [8-11]. Lysosomes, as an attractive target, participated in various physiological and signal process including intracellular transportation, protein degradation, endocytosis and cell death. Destruction of the lysosomes will result in the release of hydrolases from lysosomes to cytoplasm and induce cell death [12-14]. This means that lysosome is an ideal site for photodynamic therapy, which provided opportunities for higher cytotoxic activity against cancer cells.

Nowadays, ruthenium (Ru) complexes have aroused great interest due to their high photochemical stability, good biocompatibility and low toxicity towards normal cells [15-20]. Toward the design of photosensitizers, it is possible to regulate the solubility, targeting and optical properties of Ru complexes which was benefited from their hexa-coordinated octahedral architectures [21-24]. Among them, Ru(II)

polypyridyl complexes have been exploited as photosensitizers for PDT and chemotherapy which featured with excellent photochemical properties including photostability, intense absorbance and large Stokes shifts [25]. Besides, polypyridyl Ru complexes displayed remarkable fluorescence, which was helpful to monitor the cellular localization and investigate their anticancer mechanisms using imaging techniques [26]. It is worth mentioning that, TLD1433 ([Ru(II)(4,4'-dimethyl-2,2'-bipyridine)$_2$-(2-(2',2":5",2"'-terthiophene)-imidazo[4,5-f][1,10]phenanthroline)]$^{2+}$), as the first Ru(II)-based photosensitizer has entered clinical trials because of its good therapeutic effect against non-muscle invasive bladder cancer through PDT [27,28]. It is expected that polypyridyl Ru complexes as a new generation of photosensitizers could be used in clinical treatment of tumors [29]. On the other hand, rhein (4,5-dihydroxyanthraquinone-2-carboxylic acid), as one of the most important Chinese herbal medicines was widely used in antibacterial, anti-inflammation and anticancer applications because of its wide spectrum of pharmacological effects [30-33]. Moreover, rhein applied to animal model and displayed inhibition ability to various cancer cells growth and proliferation including human lung cancer, human breast cancer and melanoma [34]. Rhein as a quinone compound with high redox activity could produce ROS and thus induce cancer cells to death [35]. However, poor solubility and low bioavailability of rhein limited its development as potential anticancer agent. Therefore, enhancing the bioavailability of rhein would reduce the medication dose and improve the biological activities.

Herein, we designed a lysosome-targeted photosensitizer based on a polypyridyl Ru complex, **Rhein-Ru(bpy)$_3$** (bpy=2,2′-bipyridine, rhein=4,5-dihydroxy-9,10-dioxoanthracene-2-carboxylic acid), which contained a modified rhein and two bidentate ligands (Scheme S1). **Rhein-Ru(bpy)$_3$** exhibited strong fluorescence and high singlet oxygen ($^1O_2$) quantum yield, which not only help exert its anticancer effect, but also monitor the therapeutic effect using confocal imaging. Compared with rhein, **Rhein-Ru(bpy)$_3$** displayed higher solubility and thus decreased the dosage, exhibited high cytotoxicity against cancer cells by autophagy

pathway, and could overcome the drug resistance towards cisplatin-resistant cells. We hope this design will provide new insights to develop new organelle-targeting anticancer PDT agent.

2. Experimental section

2.1 Materials and methods

All the related chemicals were acquired from commercial resources, without further purification. 1-(3-dimethylaminopropyl)-3-ethylcarbodiimide hydrochloride (EDCI), 4,4'-dimethyl-2,2'-dipyridyl, SeO_2, $NaHCO_3$, $MgSO_4$, $Na_2S_2O_5$, Na_2CO_3, K_2CO_3, NaOH, LiCl, NH_4PF_6, $Ru(bpy)_3Cl_2{\cdot}6H_2O$, zinc powder, ammonium acetate, hydroxylamine hydrochloride, 1,3-diphenyliso-benzofuran (DPBF), 4,5-dihydroxyanthraquinone-2-carboxylic acid (rhein), trimethylamine (TEA), 1-hydroxybenzotriazole (HOBt), bipyridine (bpy), ruthenium(III) chloride hydrate ($RuCl_3{\cdot}3H_2O$), and the solvents used in this article were purchased from Energy Chemical. Dulbecco's modified eagle medium (DMEM), trypsin, phosphate buffered saline (PBS), fetal bovine serum (FBS), 3-(4,5-dimethyl-2-thiazolyl)-2,5-diphenyl-2H-tetrazolium bromide (MTT), Lyso Tracker Green (LTG), 4',6-diamidino-2-phenylindole (DAPI), Triton X-100, 2′,7′-dichlorofluorescin diacetate (DCFH-DA), BCA kits, propidium iodide (PI) and Annexin V-FITC were obtained from KeyGEN BioTECH. LC3 primary antibody and secondary antibody were purchased from proteintech for western blotting.

^1H NMR data were obtained on a Bruker AVANCE 400 spectrometer at room temperature. Electrospray ionization mass spectra (ESI-MS) were analyzed on LCQ spectrometer (Thermo Scientific, USA). UV-vis spectra were recorded on a Lambda 365 UV-vis spectrophotometer. Fluorescence spectra were measured using FS5 Spectrofluorometer (Edinburgh Instruments, England). Cancer cell lines were incubated in a humidified incubator (Thermo Fisher Scientific, USA). Cell viability data were collected on a microplate reader (LabServ K3, Thermo Fisher Scientific, USA). Confocal imaging experiments were carried out on confocal microscope (A1,

Nikon, Japan). Flow cytometry analysis was applied on flow cytometer (BD FACSVerse, USA). Western blotting experiments were conducted on Mini-Protean Tetra System (BIO RAD, Powerpac HC, USA), of which signal was enhanced by Tanon High-sig ECL Western Blotting substrate.

2.2 Design and Synthesis of the compounds

Synthesis of 3((4'-methyl-[2,2'-bipyridine]-4-yl) methanamine) was based on the reference with some modifications [36].

SeO_2 (1.34 g,12.1 mmol) was added to the solution of 4,4'-dimethyl-2,2'-dipyridyl (2.12 g,11.5 mmol) in 1,4-dioazne (100 mL) and heated to refluxed for 24 h. The reaction mixture was filtrated immediately to remove the insoluble solid, the solvent was removed under reduced pressure. Supersaturated $NaHCO_3$ (50 mL) was added to the residues, then extracted with dichloromethane (CH_2Cl_2, 40 mL*3), after drying over with $MgSO_4$, the organic phase was collected and evaporated. 0.3 mol/L $Na_2S_2O_5$ was added to the residues and stirred for 0.5 h, then the mixture was filtrated to remove insoluble solid. Na_2CO_3 was added to adjust the filtrate to pH=10, the product was extracted with CH_2Cl_2 (40 mL*3), then the organic phase was dry with $MgSO_4$ and evaporated to dryness and dried *in vacuum*, obtained 1 (4'-methyl-[2,2'-bipyridine]-4-carbaldehyde) as a colorless solid. Yield: 2.5 g, 46.7%.

A reaction mixture of 1 (2.5 g, 12.6 mmol), hydroxylamine hydrochloride (3 g, 44 mmol) and K_2CO_3 (8 g, 60 mmol) in methanol (MeOH, 30 mL) and water (30 mL) was stirred for 1 h at 80 ℃. After cooling to room temperature, the mixture was poured into cold water (300 mL) to form a large amount of white precipitate, then filtered and dried *in vacuum* to yield 2 (4'-methyl-[2,2'-bipyridine]-4-carbaldehyde oxime) as a white solid. Yield: 2.13 g, 83%.

Ammonium acetate (1.93 g, 25 mmol), ammonia (30 mL, 50 mmol) and H_2O (20 mL) were added to a solution of 2 (2.13 g, 10 mmol) in ethanol (20 mL), the reaction mixture was heated to reflux and stirred for 30 min. Zinc powder (2.8 g, 50 mmol) was slowly added to it and reacted for 3 h. After cooling to room temperature, it was

filtrated to remove the zinc residue. Ethanol was removed under reduced pressure. Poured NaOH (7 g, 175 mmol) into the residues, then the mixture was extracted with CH_2Cl_2 (3*100 mL). After drying over with $MgSO_4$, the solvent was removed to form a white solid. Yield: 0.96 g, 48%. ^{1}H NMR (400 MHz, Chloroform-d) δ (ppm): 8.64 (dd, J = 5.0, 0.8 Hz, 1H), 8.56 (dd, J = 5.0, 0.8 Hz, 1H), 8.36 (dd, J = 1.7, 0.9 Hz, 1H), 8.24 (tt, J = 2.4, 0.8 Hz, 1H), 7.33-7.29 (m, 1H), 7.16 (ddd, J = 5.0, 1.7, 0.8 Hz, 1H), 4.02 (s, 2H).

Synthesis of the ligand **Rhein-bpy** was as follows: To a solution of rhein (0.2874 g, 1 mmol) in DMF (N,N-dimethylformamide, 20 mL) was added EDCI (0.2112 g, 1.1 mmol) and TEA (0.2 mL). The reaction mixture was stirred at 0 ^{o}C for 20 min. Then HOBt (0.1155 g, 0.85 mmol) was added, after stirred at 0 ^{o}C for another 20 min, 3 (0.2 g, 1 mmol) was added to the mixture, the reaction was stirred at room temperature for 2 d. DMF was removed by rotary evaporation and the crude product was purified by column chromatography on silica gel (CH_2Cl_2/MeOH, 20:1 v/v) to afford a yellow solid. Yield: 168 mg, 36%. ^{1}H NMR (400 MHz, DMSO-d_6 (dimethyl sulfoxide)) δ (ppm): 11.93 (s, 2H), 9.67 (t, 1H), 8.63 (d, *J* = 5.0 Hz, 1H), 8.52 (d, *J* = 4.9 Hz, 1H), 8.38 (s, 1H), 8.24 (d, *J* = 5.0 Hz, 2H), 7.87 (s, 2H), 7.78 (s, 1H), 7.45-7.27 (m, 2H), 7.27-7.23 (m, 1H), 4.63 (d, *J* = 5.6 Hz, 2H), 2.42 (s, 3H). ^{13}C NMR (101 MHz, DMSO-d_6) δ (ppm): 165.1, 163.8, 163.5, 138.0, 137.3, 134.0, 132.6, 130.5, 129.5, 127.8, 124.9, 124.0, 123.4, 122.4, 121.8, 44.8, 18.3.

Synthesis of $Ru(bpy)_2Cl_2$ was corresponding to the reference [37].

A solution of $RuCl_3{\cdot}3H_2O$ (7.8 g, 29.8 mmol), bipyridine (9.36 g, 60 mmol) and LiCl (8.4 g, 2mmol) in DMF (50 mL) was heated to reflux and stirred for 8 h. The reaction system was in dark environment during this period. The reaction mixture was poured into acetone (250 mL) and cooled at 0 ℃ overnight after cooled to room temperature. The mixture was filtrated and obtained a dark red-violet product. The solid was washed with water (25 mL*3), ethanol (25 mL*3) and diethyl ether (25 mL*3), then it was dried *in vacuum*. Yield: 9.4 g, 78%.

Synthesis of the complex **Rhein-Ru(bpy)$_3$**: A mixture of **Rhein-bpy** (50 mg, 0.1

mmol), $Ru(bpy)_2Cl_2$ (70 mg, 0.15 mmol) and MeOH (30 mL) was stirred at 85 ^oC for 2 d under argon atmosphere. After the reaction mixture was cooled to room temperature, NH_4PF_6 (30 mg, 0.18 mmol) was added to obtain the raw product and washed three times with ethyl acetate. The crude product was purified by column chromatography on silica gel (CH_2Cl_2/MeOH, 20:1-10:1 v/v). Yield: 31.5 mg, 27%. ^1H NMR (400 MHz, DMSO-d_6) δ (ppm): 11.93 (d, *J* = 18.8 Hz, 2H), 9.61 (s, 1H), 8.83 (dd, *J* = 9.7, 5.5 Hz, 5H), 8.74 (s, 1H), 8.17 (dd, *J* = 11.8, 4.6 Hz, 5H), 7.89-7.83 (m, 2H), 7.78-7.71 (m, 5H), 7.67 (d, *J* = 5.9 Hz, 1H), 7.53 (dt, *J* = 13.0, 6.0 Hz, 5H), 7.48-7.42 (m, 2H), 7.39 (d, *J* = 5.4 Hz, 1H), 4.79-4.68 (m, 2H), 2.54 (s, 3H). Elemental Analysis (EA): calcd for [**Rhein-Ru(bpy)$_3$**]$_2PF_6$ (1169.09): C, 48.24%; H, 3.02%; N, 8.38%. Found: C, 48.35%; H, 2.92%; N, 8.34%. HRMS (positive mode, m/z): calcd 439.585, found 439.586 for [**Rhein-Ru(bpy)$_3$**]$^{2+}$. ESI-MS (positive mode, m/z): calcd 439.58, found 439.75 for [**Rhein-Ru(bpy)$_3$**]$^{2+}$.

2.3 Density functional theory (DFT) calculation

The geometry was optimized using DFT method with B3LYP functional. For Ru, lanl2DZ basis set with ECP was used, and 6-31G(d,p) was used for the nonmetal atoms. Linear response time-dependent DFT (TD-DFT) was performed to calculate the first 5 triplet excited states with 6-31+G(d,p) basis set for nonmetal atoms and lanl2DZ with ECP for Ru. All the calculations were carried out with Gaussian09 software package.

2.4 Log $P_{o/w}$ measurement

Pre-saturated PBS buffer and octanol were obtained by shaking the mixture of PBS buffer and octanol for 7 days. Pre-saturated octanol (2 mL) containing **Rhein-Ru(bpy)$_3$** (2 mg), rhein (2 mg), $Ru(bpy)_3$ (2 mg) was reacted with PBS (2 mL) in 10 mL tube, respectively. The mixture was shaken in the dark for 4 h at room temperature. The two phases were separated by centrifugation and the concentrations of compounds in the two phases were determined by spectrophotometry. The partition coefficient of the complex is calculated by the equation log $P_{o/w}$ = log (A_o/A_w), where

"A" refers to the absorbance of the complex at maximum absorption. The final results were expressed as the average of three independent experiments.

2.5 Singlet oxygen measurements

The singlet oxygen quantum yields (Φ_Δ) of **Rhein-Ru(bpy)$_3$** treated with irradiation was measured by the absorbance change of the $^1O_2$ scavenger DPBF, with $Ru(bpy)_3Cl_2 \cdot 6H_2O$ as standard (Φ_Δ=0.22 in water, 0.81 in MeOH) [38]. The **Rhein-Ru(bpy)$_3$** (10 μM) was added in the solution of DPBF (50 μM) in MeOH/PBS (1:4, v/v), the mixed solution was irradiated with 450 nm light (power: 3.5 mW cm^{-2}) for 5 s, the absorbance was measured after each irradiation. Mapping with the absorbance change of DPBF at 414 nm vs irradiation time, and the singlet oxygen quantum yields (Φ_Δ) of the complex was calculated with the following modified equation [39-41]:

$$\Phi(t) = \Phi(s) \times \frac{k(t)}{k(s)} \times \frac{F(s)}{F(t)}$$

Where 't' and 's' are the **Rhein-Ru(bpy)$_3$** and $Ru(bpy)_3Cl_2 \cdot 6H_2O$, respectively, k is the slope of the absorbance cuves of DPBF in 414 nm vs irradiation time. F is absorption correction factor, $F = 1 - 10^{-OD}$, OD is the absorbance of the solution at irradiation wavelength.

2.6 Stability study

Stability study of **Rhein-Ru(bpy)$_3$** was investigated by UV-vis absorption spectroscopy and ESI-MS spectrum. The time-dependent absorption spectra of **Rhein-Ru(bpy)$_3$** (10 μM) in cell culture media at 37 ^{o}C for 48 h and the absorbance was recorded every 3 h. The time-dependent ESI-MS spectrum of **Rhein-Ru(bpy)$_3$** in MeOH was conducted at 37 ^{o}C for 48 h.

2.7 Cellular localization

Cellular localization assays were measured by confocal laser scanning microscopy (CLSM). A549 cells were cultured at a density of 5×10^5 cells/mL and allowed to grow overnight at 37 ^{o}C. Then the cells were exposed

to **Rhein-Ru(bpy)$_3$** (10 μM) at 37 °C for 24 h in dark condition, and 150 nM Lyso Tracker Green (LTG) was added at 37 °C for another 30 min. Then the cells were washed twice with PBS and visualized by laser confocal microscope (A1, Nikon, Japan) with a 40× oil-immersion objective lens immediately. The excitation wavelengths for **Rhein-Ru(bpy)$_3$** and LTG were 488 nm, while the emission filters were 610 ± 20 nm for **Rhein-Ru(bpy)$_3$**, and 520 ± 20 nm for LTG. The images were analyzed by NIS-Elements Viewer 4.20 software.

2.8 ROS detection by flow cytometry

A549 cells were cultured in 6-well plates with a density of 1× 10^5 cells/well overnight at 37 °C. Then the medium was replaced by fresh medium contained different concentrations of **Rhein-Ru(bpy)$_3$**, after the cells were co-incubated with complex for 4 h, 15 min of irradiation (3.5 mW cm^{-2}) treated with the cells before loading ROS probe DCFH-DA. DCFH-DA (10 μM) in serum-free medium (1 mL) was added to the plates and cultured for 20 min at 37 °C, then washed twice with serum-free medium. The cells were resuspended in the PBS, and applied to the flow cytometry with excitation at 488 nm and emission at 530 nm for DCF by FL1 channel. Flow cytometry experiments were performed at BD FACSVerse Flow Cytometer (USA) and the data were analyzed by a FlowJo 7.6 software.

2.9 Cytotoxicity in vitro

MCF-7, A549, LO2, A2780 and A2780R cells were maintained in DMEM supported with 10% FBS and 1% penicillin/streptomycin. For the culturing of A549R cells, 5 μM cisplatin was added to the culture medium every two passages. All the cells were incubated in a humidified incubator at 37 °C with 5% CO_2.

We then investigated the cytotoxicities of **Rhein-Ru(bpy)$_3$,** rhein and Ru(bpy)$_3$ by MTT assays. Cells were seeded in 96-well plates at a density of 5000 cells per well and allowed to grow until the cell density reached 70%. Then the fresh medium containing different concentrations of compounds with 1% DMSO as a supporting solvent was added to each well for 48 h. Then the 5 mg/mL MTT (20 μL) was added

to each well and incubated for another 4 h at 37 °C, the medium was removed and DMSO (150 μL) was added to each well to dissolve the formed purple formazan. The absorbance at 492 nm of each well was measured by a microplate reader (LabServ K3). To test the phototoxicities of the compounds, cells were exposed to the compounds for 6 h, and with 15 min light irradiation at 450 nm (3.5 mW cm^{-2}), then continue to incubate for another 42 h.

2.10 Apoptosis analysis in A549 cells using flow cytometry

A549 cells were cultured in 6-well plates with a density of 1×10^5 cells/well overnight at 37 °C. Then the medium was replaced by fresh medium contained different concentrations of **Rhein-Ru(bpy)$_3$**, the cells were exposed to complex for 24 h, and treated with 15 min of irradiation after cultured for 6 h. A549 cells were then harvested and washed twice with cold PBS with centrifugation of 2000 rpm/5 min. A549 cells were harvested at the density of 5×10^5 cells per mL for apoptosis analysis. Then the binding buffer (0.5 mL) was added to resuspension the cells, Annexin V-FITC (5 μL) and PI (5 μL) were added respectively and cultured in 37 ^{o}C for 15 min in dark. The samples were applied to flow cytometry in 1 h with excitation at 488 nm and emission at 530 nm for Annexin V-FITC by FL1 channel, and excitation at 488 nm and emission >630 nm for PI by FL3 channel. The apoptosis data were processed into figure, the cells were divided into four parts: live (Annexin V−/PI−), early apoptotic (Annexin V+/PI−), late apoptotic (Annexin V+/PI+), and necrotic (Annexin V−/PI+) cells.

2.11 Autophagy using confocal laser scanning microscope

A549 cells were cultured at a density of 5×10^5 cells/mL and allowed to grow overnight at 37 °C. Cells were exposed to **Rhein-Ru(bpy)$_3$** (10 μM) at 37 °C for 24 h in dark and light, respectively. For cells cultured in light condition, cells were treated with irradiation (450 nm, 3.5 mW cm^{-2}) for 15 min after 6 h culture. The cells were fixed with 3.7% formaldehyde in PBS solution (750 μL) for 15 min in 37 °C, then the cells were washed three times with PBS. 0.2% Triton X-100 in PBS solution (750 μL)

was added to the plates and cultured for 15 min, then removed and the working solution of LC3 primary antibody marked by FITC (250 μL) was added and cultured for 1 h. Cells were washed three times of PBS, and incubation of horseradish peroxidase (HRP) conjugated secondary antibody (250 μL) for 30 min in dark. PBS was applied to wash the cells for three times, DAPI working solution was added to drying the nucleus of cells for 3-5 min. Cells were washed twice with PBS, and images of live cells were taken in PBS. The excitation wavelength for LC3 primary antibody was 488 nm and emission wavelength was 525± 25 nm, while the excitation wavelength for DAPI is 405 nm, emission wavelength was 450±25 nm.

2.12 Western blot assays

A549 cells (1×10^6 cells) were incubated in 10 cm petri dish overnight at 37 ^oC. Then the fresh medium containing different concentrations of **Rhein-Ru(bpy)$_3$** was added and co-incubated for 24 h. The cells were treated with 450 nm-irradiation (3.5 mW cm^{-2}) for 15 min after incubation for 6 h. Cells were washed twice with PBS and treated with trypsin for 2 min, then collected by centrifugation and washed with cold PBS for twice and mixed with loading buffer. The whole cell lysates and the protein was extracted by the kit and determined the concentrations by BCA kits. Then protein samples were applied in sodium dodecyl sulfate polyacrylamide gel electrophoresis (SDS-PAGE, 12% resolving gel and 15% stacking gel) at 80 V for 30 min then at 120 V for 1 h, and transferred to polyvinylidene difluoride membrane (PVDF) with 200 mA for 60 min. Membranes were subsequently blocked with 5% (w/v) nonfat milk powder in PBST (PBS buffer with 0.5% tween-20) for 2 h at room temperature and incubated with the LC3 polyclonal antibody (proteintech) for 1 h. The membranes were washed with PBST for 3 to 5 times. After incubation of HRP conjugated Affinipure Goat Anti-Rabbit lgG (H+L) secondary antibody (proteintech) for 1 h, the membranes were washed with PBST for 3 to 5 times, followed by ECL reagent (Tanon) and imaged with BIO RAD, Powerpac HC (USA). The images were analyzed by Image Lab software.

3. Results and discussion

3.1 Synthesis of the compounds

In order to improve the antitumor effect of Ru complex, the natural product rhein with antitumor property was selected to combine with the polypyridyl ruthenium complex with optical activity. After a series of reactions, we successful modified the one methyl group of 4,4'-dimethyl-2,2'-dipyridyl to high reactive methanamine group (compound 3). The ligand **Rhein-bpy** was synthesized with rhein and (4'-methyl-[2,2'-bipyridine]-4-yl) methanamine in DMF by amidation reaction and purification by column chromatography. The complex **Rhein-Ru(bpy)$_3$** was prepared by mixing Ru(bpy)$_2$Cl$_2$ and ligand **Rhein-bpy** in methanol at room temperature and purified through column chromatography (as shown in Scheme S1). The purified complex was characterized by NMR, EA, HRMS and ESI-MS.

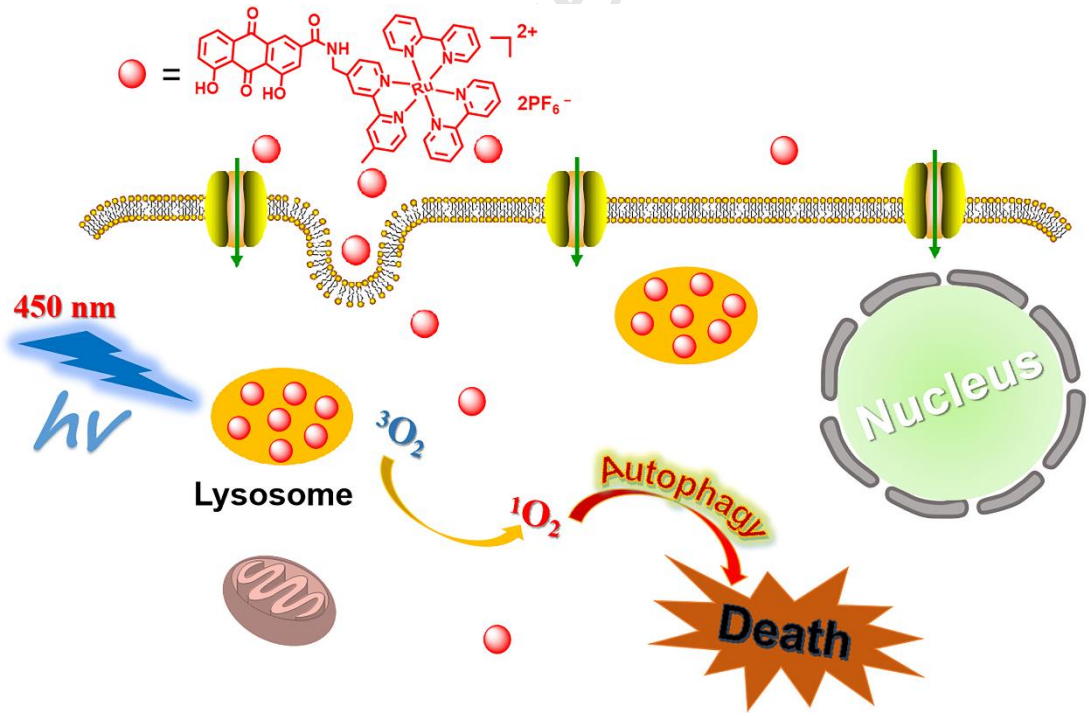

Fig. 1. Chemical structure of **Rhein-Ru(bpy)$_3$** and illustration of its photodynamic therapy in cancer treatment through autophagy pathway.

3.2 Spectral characterization

The UV-vis and fluorescence spectra of **Rhein-Ru(bpy)$_3$** (10 μM) were tested in H_2O (containing 5% DMSO) solution. As shown in Fig. 3a, the maximum absorption of complex at 450 nm, and the optical absorption properties have been further characterized with the help of DFT/TD-DFT computations. **Rhein-Ru(bpy)$_3$** features a MLCT bands at 430 and 450 nm, originating from charge transfer from the metal center to the bpy ligand according to TD-DFT calculations [42,43]. The result showed that part of electrons flowed from the metal center to the nearby ligand atoms, therefore the excitation had ^{3}MLCT character (Fig. 2). The fluorescence spectrum showed the maximum emission at 612 nm with the excitation at 450 nm, suggesting that **Rhein-Ru(bpy)$_3$** displayed a large stokes shift of 162 nm. The absorption and emission spectrum of **Rhein-Ru(bpy)$_3$** were similar to that of ligand **Rhein-bpy** (Fig. S6).

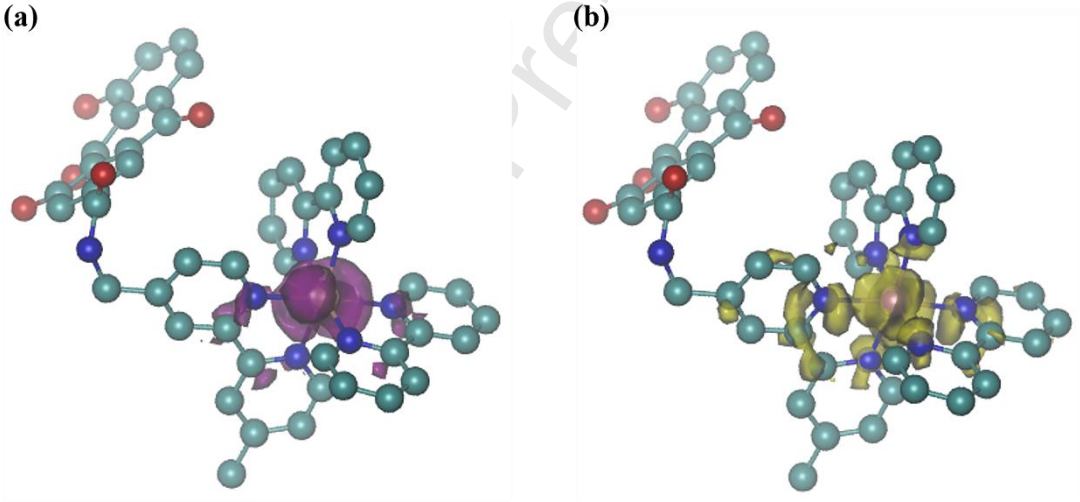

Fig. 2. The electron density difference between the triplet third excited state and ground state with absorption wavelength at 440.6 nm. Negative density difference locates in the purple range (a) and positive density difference locates in the yellow range (b). The result showed that part of electrons flowed from the metal center to the nearby ligand atoms, therefore the excitation had ^{3}MLCT character.

3.3 Partition Coefficients (log *P*)

The lipophilicity/hydrophilicity of complexes was assessed by calculated the octanol/water partition coefficient (log $P_{o/w}$) of rhein, Ru(bpy)$_3$ and **Rhein-Ru(bpy)$_3$**.

Such a coefficient is known to allow for predictions of the cell uptake efficiency, has significant effects on their cytotoxic potency [24]. The $Ru(bpy)_3$ was found to be hydrophilic with the log *P* value of -1.322 and **Rhein-Ru(bpy)$_3$** showed the log *P* value of -0.17 (Table S1), which means **Rhein-Ru(bpy)$_3$** was more lipophilic than $Ru(bpy)_3$. This might mean **Rhein-Ru(bpy)$_3$** could penetrate the lipophilic bilayer of cancer cells more easily, and exhibit higher cytotoxicity against cancer cells.

3.4 ROS generation in solution

The singlet oxygen ($^1O_2$) quantum yields (Φ_Δ) of the complex treated with irradiation was measured by the absorbance change of the $^1O_2$ scavenger DPBF [40], with $Ru(bpy)_3Cl_2{\cdot}6H_2O$ as the standard. When treated with 10 μM **Rhein-Ru(bpy)$_3$** upon 450 nm irradiation, the absorbance of DPBF in 414 nm was decreased, indicated that DPBF was degraded by $^1O_2$ (Fig. 3b). The $^1O_2$ quantum yields (Φ_Δ) of the complex was calculated as 0.184 in water, 0.679 in methanol, which is slightly lower than that of $Ru(bpy)_3Cl_2{\cdot}6H_2O$ (Φ_Δ=0.22 in water, 0.81 in MeOH) [41]. This means the **Rhein-Ru(bpy)$_3$** could produce ROS with light irradiation with high yields and function as a photosensitizer to kill the cancer cells.

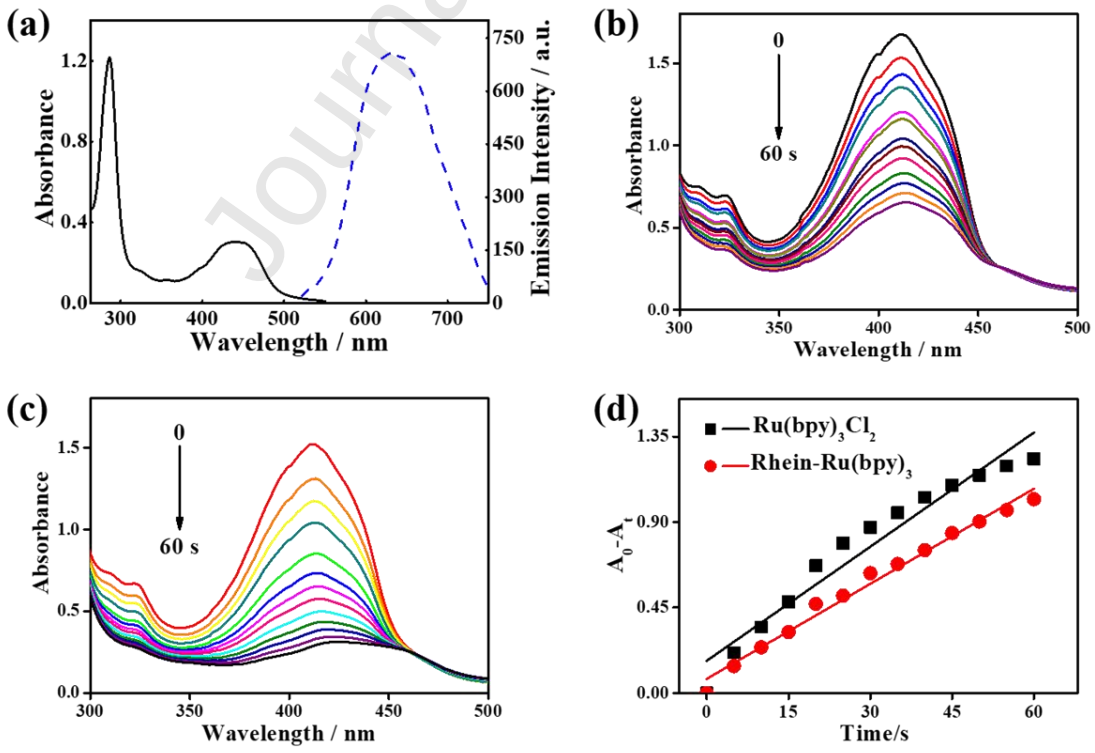

Fig. 3. (a) UV-vis absorption spectrum (black line) and emission spectrum (blue dotted line) of **Rhein-Ru(bpy)$_3$** (10 μM) in H_2O solution (containing 5% DMSO), λ_{ex} = 450 nm. Changes in the absorption spectra of DPBF solution (50 μM) in the presence of 10 μM **Rhein-Ru(bpy)$_3$** (b) and $Ru(bpy)_3Cl_2 \cdot 6H_2O$ (c) in MeOH/PBS (1/4 v/v) solution irradiated by a 450 nm laser with a light power density of 3.5 mW cm^{-2}; (d) Comparative plots of In (A_0-A_t) as a function of time. A_0 is the initial absorbance, and A_t is the absorbance at different irradiation times (0-60 s).

3.5 Stability study

The stability of **Rhein-Ru(bpy)$_3$** was analyzed by UV-vis absorption spectroscopy and ESI-MS spectrum. The time-dependent absorption spectra of **Rhein-Ru(bpy)$_3$** in cell culture media at 37 ^{o}C were shown in Fig. S7. Negligible changes in the absorption spectra of **Rhein-Ru(bpy)$_3$** both under light and dark conditions were observed over 48 h, which suggested that the complex was stable in the PDT process. Besides, we detected the ESI-MS of **Rhein-Ru(bpy)$_3$** under light and dark conditions to confirm the stability of the complex. As shown in Fig. S8, only 1 positive-ion peak at 439.67(58) was observed in dark and light conditions, which is consistent with the molecular ion peak of **Rhein-Ru(bpy)$_3$** in methanol solution (Fig. S4). This again proved that the complex was stable in the PDT process. And the results were consistent with the previous literature that photosensitizer itself is not changed during PDT process, it merely acts as an ‘‘energy relay” to absorb light and transfer energy [44].

3.6 Cellular localization by confocal imaging

The cellular localization of **Rhein-Ru(bpy)$_3$** was further investigated by CLSM in lung cancer A549 cells. As shown in Fig. 4, **Rhein-Ru(bpy)$_3$** showed red fluorescence within cells under excitation, the signal of Ru complex overlapped well with the commercial lysosome dye LTG with the Pearson correlation coefficient of ~0.83 (Fig. 4). This suggested that **Rhein-Ru(bpy)$_3$** mainly accumulated in the lysosomal organelles. As is reported that cellular targeting of complex was related to the several factors such as hydrophobicity, type and number of charges. Considering

the lipophilicity and negative potential of the mitochondrial outer membrane, the most mitochondria-targeting metal complexes that have been developed are lipophilic cations. While lysosomes are the final destinations of endocytosis, this process can be used to selectively target metal complexes to lysosomes, some hydrophilic cationic metal complexes, which cannot freely diffuse into cells, can also be transported into lysosomes by endocytosis. which could be assigned to **Rhein-Ru(bpy)$_3$** was hydrophilic (Table S1) and selectively targeted to lysosomes by endocytosis [45,46]. Whereas, Ru(bpy)$_3$ exhibited poor targeting property, it was not concentrated in organelles but distributed in whole cell in small amount [24].

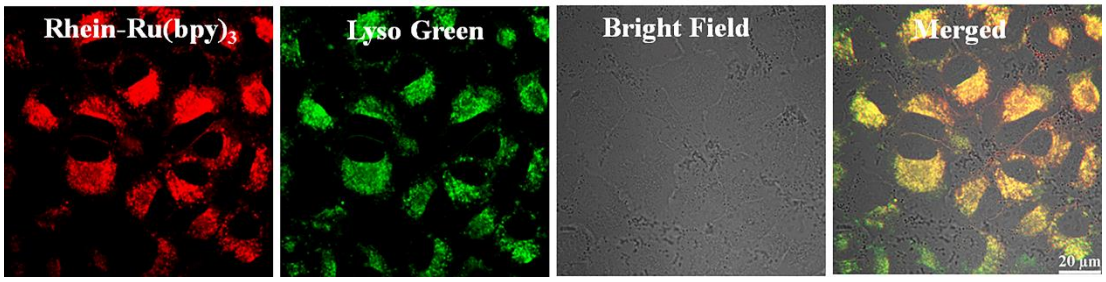

Fig. 4. Confocal imagings of the intracellular fluorescence in A549 cells exposed to **Rhein-Ru(bpy)$_3$** (10 μM) for 24 h, and localized with LysoTracker Green; λ_{ex}: 488 nm; λ_{em}: 590 nm-630 nm for **Rhein-Ru(bpy)$_3$**; λ_{ex}: 488 nm; λ_{em}: 500 nm-540 nm for Lyso Tracker Green; Scale bar: 20 μm. The **Rhein-Ru(bpy)$_3$** mainly accumulated in lysosomes.

3.7 ROS generation in in living cells

We further investigated the intracellular ROS generation of **Rhein-Ru(bpy)$_3$** upon light irradiation by flow cytometry, using DCFH-DA as the fluorescence probe for ROS detection [47]. Fig. 5a showed that the fluorescence signal of DCF was very weak in the dark incubation of **Rhein-Ru(bpy)$_3$** and the intensity remained unchanged with the increment of **Rhein-Ru(bpy)$_3$** concentration, suggesting that **Rhein-Ru(bpy)$_3$** could not generate ROS in dark condition. While the fluorescence intensity increased apparently with the increased concentration of **Rhein-Ru(bpy)$_3$** (0~20 μM) when treated with 15 min of light irradiation (3.5 mW cm^{-2}, Fig. 5b, 5c). This suggested that the complex **Rhein-Ru(bpy)$_3$** could produce ROS in cancer cells when treated with light irradiation, which might help exert its photodynamic therapy towards cancer cells.

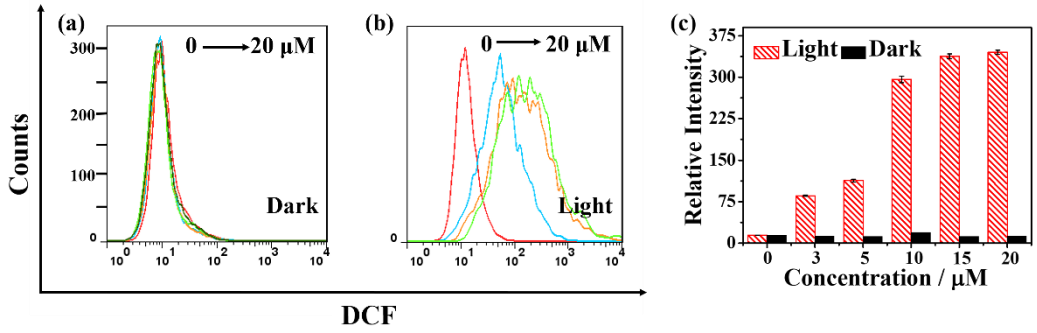

Fig. 5. Cellular ROS detection using DCFH-DA (10 μM) as the fluorescent probe by flow cytometry, incubated with **Rhein-Ru(bpy)$_3$** for 4 h in the dark (a) and with 15 min light irradiation (450 nm, 3.5 mW cm^{-2}) (b) λ_{ex}= 488 nm, λ_{em}=510-540 nm. The complex treated with irradiation could produce ROS in cancer cells. (c) Relative fluorescence intensity of DCF in A549 cells treated with **Rhein-Ru(bpy)$_3$** in dark and light condition at different concentrations of 0~20 μM, the histogram showed the level of ROS induction in A549 cancer cells treated with **Rhein-Ru(bpy)$_3$**. Data were quoted as the mean ±SD of three replicates.

3.8 Cytotoxicity *in vitro*

The cytotoxicity of **Rhein-Ru(bpy)$_3$** was investigated against different cancer cells by MTT assays. Tumor cell lines MCF-7, A549, NB-4, A2780, cisplatin resistant A2780 cells (A2780R) and human normal liver cells (LO2) were exposed to culture containing different concentrations of **Rhein-Ru(bpy)$_3$** for 48 h, of which were irradiation with 450 nm lamp for 15 min after the drugs were cultured with cells for 6 h. The cell lines incubated with **Rhein-Ru(bpy)$_3$** in dark condition without light irradiation were used as the control groups to verify the effectiveness of PDT. As expected, the complex exhibited apparent phototoxicity and poor dark cytotoxicity towards the different cell lines. The IC_{50} values of **Rhein-Ru(bpy)$_3$** toward A2780 cells were ~49.3 and ~5.2 μM in dark and light condition, separately. The phototoxicity index (PI) was the ratio between the IC_{50} values in the dark upon light irradiation was up to 9.5-fold, indicating that the cytotoxicity highly enhanced after 15 min-irradiation compared to that of dark incubation. Similarly, the anticancer activity of **Rhein-Ru(bpy)$_3$** against A2780R, A549, MCF-7 and LO2 cells also showed poor cytotoxicity in dark incubation, with the IC_{50} values of ~91.3, ~64.7, ~250.6 and ~35.1 μM, respectively. While the cytotoxicity increased dramatically after 15 min-irradiation treatment, the IC_{50} values decreased to ~3.2, ~2.4, ~7.6 and ~8.7 μM, respectively, again proved the high photocytotoxicity of the complex **Rhein-Ru(bpy)$_3$**. **Rhein-Ru(bpy)$_3$** showed high photocytotoxicity for all the tested cancer cells, indicating the complex exhibited universality to kill various tumors as a potential PDT agent. Moreover, **Rhein-Ru(bpy)$_3$** showed higher cytotoxicity

whatever in dark or light condition compared to $Ru(bpy)_3$ (Table 1). The higher anticancer efficacy of **Rhein-Ru(bpy)$_3$** than the $Ru(bpy)_3$ could be explained by its higher cellular uptake efficiency [24]. Strikingly, **Rhein-Ru(bpy)$_3$** displayed much higher efficacy against A2780R cells than that of cisplatin, with the PI value up to ~28.5 times, which meant that **Rhein-Ru(bpy)$_3$** might overcome the cisplatin resistance of A2780R cells.

Table 1. IC_{50} values of **Rhein-Ru(bpy)$_3$**, rhein, $Ru(bpy)_3$ and cisplatin against different cell lines both in dark and light (the cell lines exposed to **Rhein-Ru(bpy)$_3$** for 6 h in dark and irradiated with 450 nm light for 15 min, 3.5 mW cm^{-2}) conditions.

complex		IC_{50} value (μM) towards different cell lines				
		A2780	A2780R	A549	MCF-7	LO2
Rhein-Ru(bpy)$_3$	dark	49.3±1.1	91.3±2.2	64.7±0.3	250.6±0.2	35.1±6.2
	light	5.2±1.1	3.2±0.1	2.4±0.02	8.1±0.3	8.7±0.2
	PI[a]	9.5	28.5	26.9	20.9	4.0
Rhein	dark	126.9±4.7	116.5±6.3	130.6±6.2	>100	123.8±6.1
	light	>100	129.9±6.7	144.8±3.1	>100	144.7±2.0
$Ru(bpy)_3$	dark	>200	>200	>200	>200	>200
	light	>200	>200	>200	>200	>200
cisplatin		3.2±0.0	18.0±0.4	13.9±0.2	14.4±0.1	10.1±0.1

[a] The PI (phototoxicity index) was the ratio between the IC_{50} values in the dark upon light irradiation.

3.9 Mechanism of cell death

The effect of complex **Rhein-Ru(bpy)$_3$** on apoptosis of A549 cells was studied by flow cytometry. Cells were divided into four parts: Q1 region, necrotic cells

(Annexin V−/PI+); Q2, late apoptotic cells (Annexin V+/PI+); Q3, early apoptotic cells (Annexin V+/PI−) and Q4, living (Annexin V−/PI−) cells [48]. As shown in Fig. S9, with the increase of the concentration of **Rhein-Ru(bpy)$_3$**, the cells were mainly concentrated in the living cell region of Q4, the proportion was up to 85% with no obvious fluctuation, and other regions have showed negligible changes as well. Apoptosis data exhibited that the complex **Rhein-Ru(bpy)$_3$** induced cancer cells to death by not apoptosis but other pathways.

Based on the above results, we further studied the mechanism of cell death after treated with **Rhein-Ru(bpy)$_3$**. To our knowledge, autophagy is a lysosomal degradation pathway, the enhanced of reactive oxygen species might induce the cell death through autophagy mechanism [49,50]. To confirm the autophagy induced by **Rhein-Ru(bpy)$_3$**, confocal laser scanning microscope was applied to observe the fluorescence of GFP-LC3 fusion protein in A549 cells and monitor the process of autophagy. GFP-LC3 fusion protein was diffused in cytoplasm without autophagy, and no fluorescence could be observed. While occurrence of autophagy would induce the GFP-LC3 fusion protein transferring to AV (autophagosomal vacuoles) membrane, light green fluorescence spots could be observed by fluorescence microscope [51]. As shown in Fig. 6a, there was no green fluorescence spot when the cells were incubated with **Rhein-Ru(bpy)$_3$** in dark condition, indicating the dark incubation cannot induce the autophagy of cancer cells. While A549 cells exposed to **Rhein-Ru(bpy)$_3$** for 6 h in dark and irradiated with 450 nm light for another 15 min, green spots were observed around the nucleus, which suggested that the cells underwent obvious autophagy after treated with **Rhein-Ru(bpy)$_3$** in light condition.

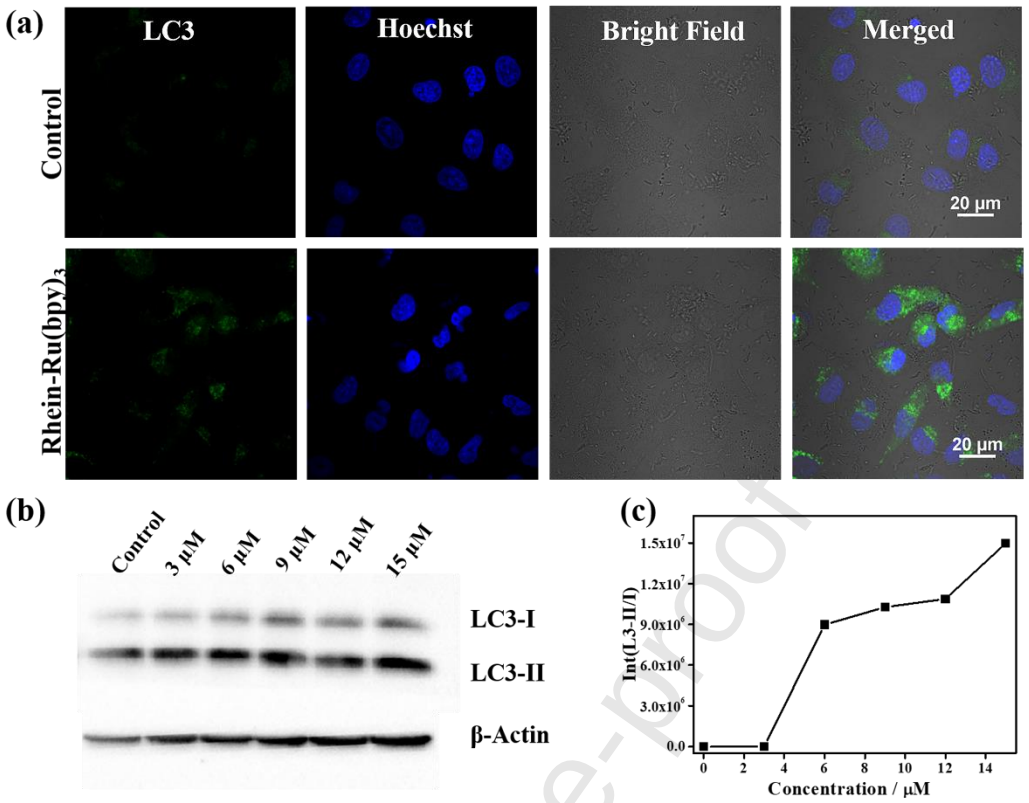

Fig. 6. (a) Confocal imagings of the intracellular fluorescence in A549 cells exposed to **Rhein-Ru(bpy)$_3$** (10 μM) for 24 h in dark and in light, treated with irradiation (15 min, 450 nm, 3.5 mW cm^{-2}) after 6 h of incubation; λ_{ex}: 488 nm; λ_{em}: 520-530 nm for LC3; λ_{ex}: 405 nm; λ_{em}: 454 nm for DAPI; Scale bar: 20 μm; (b) LC3 expression in A549 cells after exposed to **Rhein-Ru(bpy)$_3$** for 24 h in light, treated with 450 nm light irradiation for 15 min after 6 h-incubation. (c) The ratio of LC3-II/I treated with **Rhein-Ru(bpy)$_3$** at different concentrations of 3~15 μM.

To further validated the autophagy caused by **Rhein-Ru(bpy)$_3$**, we used western blotting assay to analyze the change of autophagy-related protein concentration. Map1LC3, also known as LC3, is the mammalian homologue of yeast Apg8 and is involved in the formation of autophagosomal vacuoles [52]. As shown in Fig. 6b, the level of LC3-II (16 KDa) was apparently increased along with the enhanced concentration of **Rhein-Ru(bpy)$_3$**, with β-actin (43 KDa) as the standard reference. Once autophagy occurred, cytoplasmic form LC3-I will remove a small segment of polypeptide by zymolysis, and transform to autophagosome membrane of LC3-II. The level of autophagy can be measured by calculating the ratio of LC3-II to LC3-I using

Image Lab software. As shown in Fig. 6c, the ratio of LC3-II to LC3-I is increased with the increased concentration of **Rhein-Ru(bpy)$_3$**, existing a dose-dependent relationship between the concentration of the complex and autophagy level (Fig. 6c). Above all, western blotting assay and fluorescence imaging results confirmed that **Rhein-Ru(bpy)$_3$** irradiated with 450 nm light will induce cancer cells to death by the autophagy pathway.

4. Conclusion

In summary, we synthesized a polypyridyl Ru(II) complex **Rhein-Ru(bpy)$_3$** with lysosome-targeted characteristics and high singlet oxygen quantum yield. As a potential PDT agent, **Rhein-Ru(bpy)$_3$** exhibited poor cytotoxicity in dark and high phototoxicity with short time of irradiation, which was helpful to reduce the toxicity to normal cells. Furthermore, **Rhein-Ru(bpy)$_3$** showed high cytotoxic activity towards cisplatin-resistant A2780R cells under light conditions, which meant that the complex can overcome the cisplatin resistance during cancer therapy. Besides, **Rhein-Ru(bpy)$_3$** would induce cell death by the autophagy pathway. This design provided useful strategy and ideas for the future development of photosensitizers to reduce the toxic effects on normal cells and overcome the cisplatin resistance.

Acknowledgements

We appreciate the financial support from the National Natural Science Foundation of China (No. 21420102002, 21771109, 21778033, 21807060), the Natural Science Foundation of Jiangsu Province (No. BK20171472) and China Postdoctoral Science Foundation (No. 2019M651874).

Conflicts of Interest

There are no conflicts to declare.

References

[1] C. Imberti, P.Y. Zhang, H.Y. Huang, P.J. Sadler, New designs for phototherapeutic transition metal complexes, Angew. Chem. Int. Ed. 59 (2020) 61-73.

[2] C. Mari, V. Pierroz, S. Ferrari, G. Gasser, Combination of Ru(II) complexes and light: new frontiers in cancer therapy, Chem. Sci. 6 (2015) 2660-2686.

[3] S. Monro, K.L. Colon, H.M. Yin, J. Roque III, P. Konda, S. Gujar, R.P. Thummel, L. Lilge, C.G. Cameron, S.A. McFarland, Transition metal complexes and photodynamic therapy from a tumor-centered approach: challenges, opportunities, and highlights from the development of TLD1433, Chem. Rev. 119 (2019) 797-828.

[4] J.P. Liu, C. Zhang, T.W. Rees, L.B. Ke, L.N. Ji, H. Chao, Harnessing ruthenium(II) as photodynamic agents: encouraging advances in cancer therapy, Coordin. Chem. Rev. 363 (2018) 17-28.

[5] W.B. Hu, T.C. He, H. Zhao, H.J. Tao, R.F. Chen, L. Jin, J.Z. Li, Q.L. Fan, W. Huang, A. Baev, P.N. Prasad, Stimuli-responsive reversible switching of intersystem crossing in pure organic material for smart photodynamic therapy, Angew. Chem. Int. Ed. 58 (2019) 11105-11111.

[6] S.F. Wang, H.W. Liao, F.Y. Li, D.S. Ling, A mini-review and perspective on ferroptosis-inducing strategies in cancer therapy, Chinese Chem. Lett. 30 (2019) 847-852.

[7] J.H. Liang, Y. Zheng, X.W. Wu, C.P. Tan, L.N. Ji, Z.W. Mao, A tailored multifunctional anticancer nanodelivery system for ruthenium-based photosensitizers: tumor microenvironment adaption and remodeling, Adv. Sci. 7 (2020) 1901992.

[8] S. Chakrabortty, B.K. Agrawalla, A. Stumper, N.M. Vegi, S. Fischer, C. Reichardt, M. Kogler, B. Dietzek, M. Feuring-Buske, C. Buske, S. Rau, T. Weil, Mitochondria targeted protein-ruthenium photosensitizer for efficient photodynamic applications, J. Am. Chem. Soc. 139 (2017) 2512-2519.

[9] L. He, Y. Li, C.P. Tan, R.R. Ye, M.H. Chen, J.J. Cao, L.N. Ji, Z.W. Mao, Cyclometalated iridium(III) complexes as lysosome-targeted photodynamic anticancer and real-time tracking agents, Chem. Sci. 6 (2015) 5409-5418.

[10] H.Y. Huang, S. Banerjee, P.J. Sadler, Recent advances in the design of targeted iridium(III) photosensitizers for photodynamic therapy, ChemBioChem 19 (2018) 1574-1589.

[11] V. Venkatesh, R.B. Martin, C.J. Wedge, I.R. Canelon, C.S. Cano, J.I. Song, J.P.C. Coverdale, P.Y. Zhang, G.J. Clarkson, A. Habtemariam, S.W. Magennis,

R.J. Deeth, P.J. Sadler, Mitochondria-targeted spin-labelled luminescent iridium anticancer complexes, Chem. Sci. 8 (2017) 8271-8278.

[12] Z.Z. Tian, J.J. Li, S.M. Zhang, Z.S. Xu, Y.L. Yang, D.L. Kong, H.R. Zhang, X.X. Ge, J.M. Zhang, Z. Liu, Lysosome-targeted chemotherapeutics: half-sandwich ruthenium(II) complexes that are selectively toxic to cancer cells, Inorg. Chem. 57 (2018) 10498-10502.

[13] W.L. Ma, X.X. Ge, L.H. Guo, S.M. Zhang, J.J. Li, X.D. He, Z. Liu, Bichromophoric anticancer drug: targeting lysosome with rhodamine modified cyclometalated iridium(III) complexes, Dyes and Pigments 162 (2019) 385-393.

[14] X.L. Xue, C.G. Qian, H.B. Fang, H.K. Liu, H. Yuan, Z.J. Guo, Y. Bai, W.J. He, Photoactivated lysosomal escape of a monofunctional Pt^{II} complex Pt-BDPA for nucleus access, Angew. Chem. Int. Ed. 58 (2019) 12661-12666.

[15] P.Y. Zhang, P.J. Sadler, Advances in the design of organometallic anticancer complexes, J. Organomet. Chem. 839 (2017) 5-14.

[16] L.L. Zeng, P. Gupta, Y.L. Chen, E.J. Wang, L.N. Ji, H. Chao, Z.S. Chen, The development of anticancer ruthenium(II) complexes: from single molecule compounds to nanomaterials, Chem. Soc. Rev. 46 (2017) 5771-5804.

[17] J. Li, P.P. Zhang, Y. Xu, Z. Su, Y. Qian, S.L. Li, T. Yu, P.J. Sadler, H.K. Liu, A novel strategy to construct Janus metallamacrocycles with both a Ru-arene face and an imidazolium face, Dalton Trans. 46 (2017) 16205-16215.

[18] H.K. Liu, S.J. Berners-Price, F.Y. Wang, J.A. Parkinson, J.J. Xu, J. Bella, P.J. Sadler, Diversity in guanine-selective DNA binding modes for an organometallic ruthenium arene complex, Angew. Chem. Int. Ed. 45 (2006) 8153-8156.

[19] H.K. Liu, P.J. Sadler, Metal complexes as DNA intercalators, Acc. Chem. Res. 44 (2011) 349-359.

[20] H. Huang, K.M. Cao, Y.Q. Kong, S.M. Yuan, H.K. Liu, Y.C. Wang, Y.Z. Liu, A dual functional ruthenium arene complex induces differentiation and apoptosis of acute promyelocytic leukemia cells, Chem. Sci. 10 (2019) 9721-9728.

[21] V. Pierroz, T. Joshi, A. Leonidova, C. Mari, J. Schur, I. Ott, L. Spiccia, S. Ferrari, G. Gasser, Molecular and cellular characterization of the biological effects of ruthenium(II) complexes incorporating 2- pyridyl-2-pyrimidine-4-carboxylic acid, J. Am. Chem. Soc. 134 (2012) 20376-20387.

[22] W.L. Ma, S.M. Zhang, Z.Z. Tian, Z.S. Xu, Y.J. Zhang, X.R. Xia, X.B. Chen, Z. Liu, Potential anticancer agent for selective damage to mitochondria or lysosomes: Naphthalimide-modified fluorescent biomarker half-sandwich iridium(III) and ruthenium(II) complexes, Eur. J. Med. Chem. 181 (2019) 111599.

[23] Q. Du, L.H. Guo, X.X. Ge, L.P. Zhao, Z.Z. Tian, X.C. Liu, F.J. Zhang, Z. Liu, Serendipitous synthesis of five-coordinated half-sandwich aminoimine iridium(III) and ruthenium(II) complexes and their application as potent anticancer agents, Inorg. Chem. 58 (2019) 5956-5965.

[24] H.Y. Huang, B.L. Yu, P.Y. Zhang, J.J. Huang, Y. Chen, G. Gasser, L.N. Ji, H. Chao, Highly charged ruthenium(II) polypyridyl complexes as lysosome-localized photosensitizers for two-photon photodynamic therapy, Angew. Chem. Int. Ed. 54 (2015) 14049-14052.

[25] H.Y. Huang, P.Y. Zhang, B.L. Yu, C.Z. Jin, L.N. Ji, H. Chao, Synthesis, characterization and biological evaluation of mixed-ligand ruthenium(II) complexes for photodynamic therapy, Dalton Trans. 44 (2015) 17335-17345.

[26] Y. Zheng, D.Y. Zhang, H. Zhang, J.J. Cao, C.P. Tan, L.N. Ji, Z.W. Mao, Photo-damaging of mitochondrial DNA to overcome cisplatin resistance by a Ru-II-Pt-II bimetallic complex, Chem. Eur. J. 24 (2018) 18971-18980.

[27] S. Thota, D.A. Rodrigues, D.C. Crans, E.J. Barreiro, Ru(II) compounds: next-generation anticancer metallotherapeutics?, J. Med. Chem. 61 (2018) 5805-5821.

[28] D.A. Smithen, H.M. Yin, M.H. Beh, M. Hetu, T.S. Cameron, S.A. McFarland, A. Thompson, Synthesis and photobiological activity of Ru(II) dyads derived from pyrrole-2-carboxylate thionoesters, Inorg. Chem. 56 (2017) 4121-4132.

[29] C. Mari, V. Pierroz, S. Ferrarib, G. Gasser, Combination of Ru(II) complexes and light: new frontiers in cancer therapy, Chem. Sci. 6 (2015) 2660-2686.

[30] Q.Z. Dai, J.W. Chen, C.M. Gao, Q.S. Sun, Z.G. Yuan, Y.Y. Jiang, Design, synthesis and biological evaluation of novel phthalazinone acridine derivatives as dual PARP and Topo inhibitors for potential anticancer agents, Chinese Chem. Lett. 31 (2020) 404-408.

[31] L.W. Min, Targeting apoptosis pathways in cancer by Chinese medicine, Cancer Lett. 332 (2013) 304-312.

[32] L.T. You, X.X. Dong, X.B. Yin, C.J. Yang, X. Leng, W.P. Wang, J. Ni, Rhein induces cell death in HepaRG cells through cell cycle arrest and apoptotic pathway, Int. J. Mol. Sci. 19 (2018) 1060-1073.

[33] C.H. Huang, W.H. Chan, Rhein induces oxidative stress and apoptosis in mouse blastocysts and has immunotoxic effects during embryonic development, Int. J. Mol. Sci. 18 (2017) 2018-2035.

[34] S.W. Ip, Y.S. Weng, S.Y. Lin, D.Y. Mei, N.Y. Tang, C.C. Su, J.G. Chung, The role of Ca^{+2} on rhein-induced apoptosis in human cervical cancer Ca Ski cells, Anticancer Res. 27 (2007) 379-389.

[35] H.D. Smolarz, M. Swatko-Ossor, G. Ginalska, E. Medyńska, Antimycobacterial effect of extract and its components from rheum rhaponticum, J. AOAC Int. 96 (2013) 155-160.

[36] C. Busche, P. Comba, A. Mayboroda, H. Wadepohl, Novel Ru^{II} complexes with bispidine- based bridging ligands: luminescence sensing and photocatalytic properties, Eur. J. Inorg. Chem. 2010 (2010) 1295-1302.

[37] J. Li, X.C. Li, G.H. Xu, Z.H. Zheng, J.N. Deng, X.B. Ding, A self-deformable gel system with asymmetric shape change based on a gradient structure, Chem. Commun. 54 (2018) 11594-11597.

[38] A.A. Abdel-Shafi, P.D. Beer, R.J. Mortimer, F. Wilkinson, Photosensitized generation of singlet oxygen from vinyl linked benzo-crown-ether-bipyridyl ruthenium(II) complexes, J. Phys. Chem. A. 104 (2000) 192-202.

[39] J.P. Liu, Y. Chen, G.Y. Li, P.Y. Zhang, C.Z. Jin, L.L. Zeng, L.N. Ji, H. Chao, Ruthenium(II) polypyridyl complexes as mitochondria-targeted two-photon photodynamic anticancer agents, Biomaterials 56 (2015) 140-153.

[40] F.F. Xue, Y. Lu, Z.G. Zhou, M. Shi, Y.P. Yan, H. Yang, S.P. Yang, Two in one: luminescence imaging and 730 nm continuous wave laser driven photodynamic therapy of iridium complexes, Organometallics 34 (2015) 73-77.

[41] Y.C. Yang, Q.L. Guo, H.C. Chen, Z.K. Zhou, Z.J. Guo, Z. Shen, Thienopyrrole-expanded BODIPY as a potential NIR photosensitizer for photodynamic therapy, Chem. Commun. 49 (2013) 3940-3942.

[42] S.A Hua, M. Cattaneo, M. Oelschlegel, M. Heindl, L. Schmid, S. Dechert, O.S. Wenger, I. Siewert, L. Gonzalez, F. Meyer, Electrochemical and photophysical

properties of Ruthenium(II) complexes equipped with sulfurated bipyridine ligands, Inorg. Chem. 59 (2020) 4972-4984.

[43] A. Bonfiglio, K. Magra, C. Cebrián, F. Polo, P.C. Gros, P. Mercandelli, M. Mauro, Red-emitting neutral rhenium(I) complexes bearing a pyridyl pyridoannelated N-heterocyclic carbine, Dalton Trans. 49 (2020) 3102-3111.

[44] L.K. McKenzie, H.E. Bryant, J.A. Weinstein, Transition metal complexes as photosensitisers in one- and two-photon photodynamic therapy, Coord. Chem. Rev. 379 (2019) 2-29.

[45] K.Q. Qiu, Y. Chen, T.W. Rees, L.N. Ji, H. Chao, Organelle-targeting metal complexes: from molecular design to bio-applications, Coord. Chem. Rev. 378 (2019) 66-86.

[46] K.Q. Qiu, H.Y. Zhu, T.W. Rees, L.N. Ji, Q.L. Zhang H. Chao, Recent advances in lysosome-targeting luminescent transition metal complexes, Coord. Chem. Rev. 398 (2019) 113010.

[47] M.S. Shim, Y.N. Xia, A reactive oxygen species (ROS)-responsive polymer for safe, efficient, and targeted gene delivery in cancer cells, Angew. Chem. Int. Ed. 52 (2013) 6926-6929.

[48] Z.Z. Zhu, Z.H. Wang, C.L. Zhang, Y.J. Wang, H.M. Zhang, Z.J. Gan, Z.J. Guo, X.Y. Wang, Mitochondrion-targeted platinum complexes suppressing lung cancer through multiple pathways involving energy metabolism, Chem. Sci. 10 (2019) 3089-3095.

[49] Z.J. Yang, C.E. Chee, S. Huang, F. Sinicrope, Autophagy modulation for cancer therapy, Cancer Biol. Ther. 11 (2011) 169-176.

[50] Z.F. Yang, D. J. Klionsky, Eaten alive: a history of macroautophagy, Nat. Cell Biol. 12 (2010) 814-822.

[51] L. He, C.P. Tan, R.R. Ye, Y.Z. Zhao, Y.H. Liu, Q. Zhao, L.N. Ji, Z.W. Mao, Theranostic iridium(III) complexes as one- and two-photon phosphorescent trackers to monitor autophagic lysosomes, Angew. Chem. Int. Ed. 53 (2014) 12137-12141.

[52] W.J. Guo, Y.M. Zhang, L. Zhang, B. Huang, F.F. Tao, W. Chen, Z.J. Guo, Q. Xu, Y. Sun, Novel monofunctional platinum(II) complex Mono-Pt induces apoptosis-independent autophagic cell death in human ovarian carcinoma cells, distinct from cisplatin, Autophagy 9 (2013) 996-1008.

Declaration of interests

☑The authors declare that they have no known competing financial interests or personal relationships that could have appeared to influence the work reported in this paper.

☐The authors declare the following financial interests/personal relationships which may be considered as potential competing interests:

Graphical Abstract

A lysosome-targeted ruthenium(II) polypyridyl complex as photodynamic anticancer agent

Jun Chen [a,b], Qin Tao [b], Jian Wu [b], Mengmeng Wang [b], Zhi Su [b], Yong Qian [b], Tao Yu [c], Yan Wang [a,*], Xuling Xue [b,*] and Hong-Ke Liu [b,*]

[a] *Anhui Key Laboratory of Functional Coordination Compounds, School of Chemistry and Chemical Engineering, Anqing Normal University, Anqing 246011, China*
[b] *Jiangsu Collaborative Innovation Center of Biomedical Functional Materials, College of Chemistry and Materials Science, Nanjing Normal University, Nanjing, 210023, China*
[c] *Department of Chemistry, University of North Dakota, 151 Cornell St., Grand Forks, North Dakota, USA, 58202*
[*] *E-mail*: njwangy@live.com; xuexuling87@163.com; liuhongke@njnu.edu.cn.

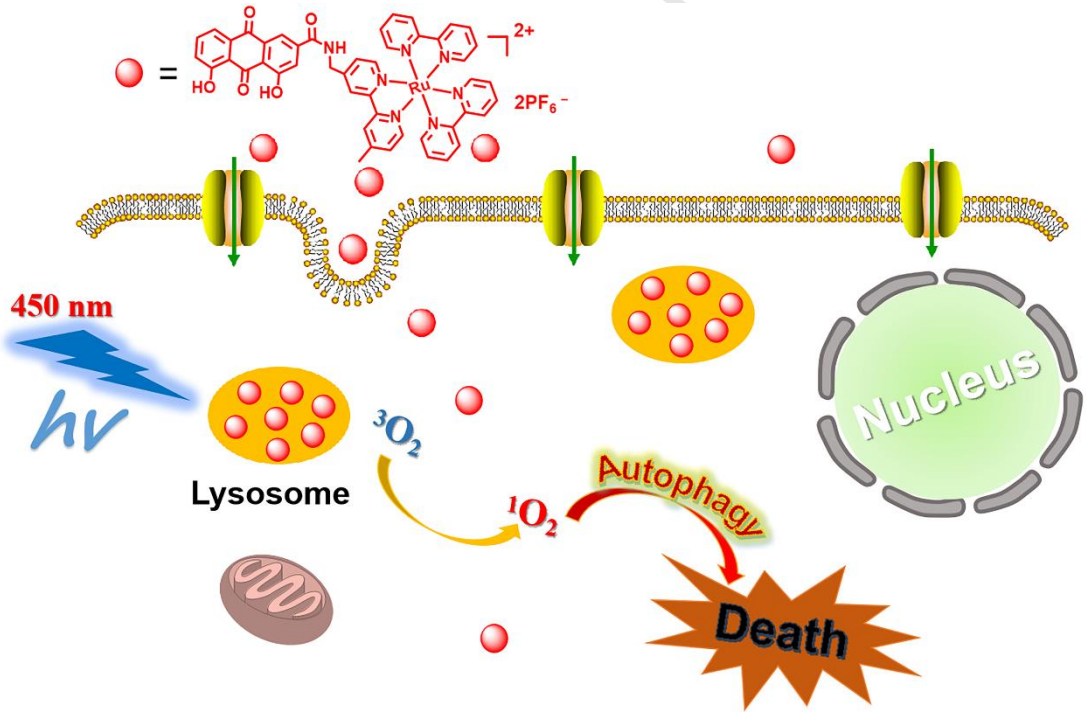

A lysosome-targeted photodynamic anticancer agent polypyridyl ruthenium complex **Rhein-Ru(bpy)$_3$** (bpy=2,2′-bipyridine, rhein=4,5-dihydroxy-9,10-dioxoanthracene-2-carboxylic acid) induces cancer cell death under light irradiation through the autophagy pathway.

Highlight

Lysosome-targeted; High phototoxicity; No drug resistance; High lipophilicity; Autophagy.

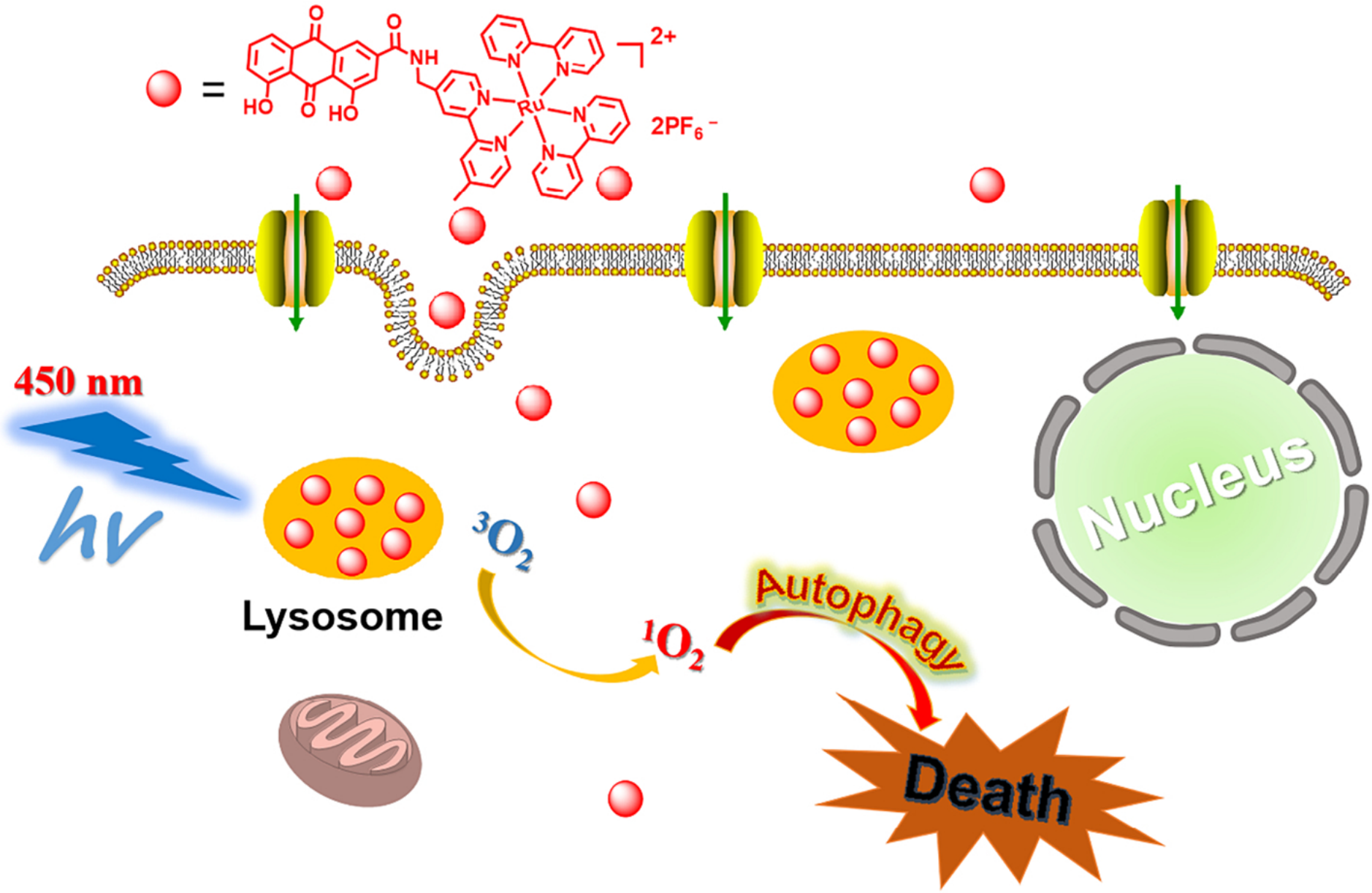
450 nm
hv
Lysosome
$^3O_2$
$^1O_2$
Autophagy
Death
Nucleus
HO
O
HO
NH
N
Ru
2+
$2PF_6^-$

Figure 1

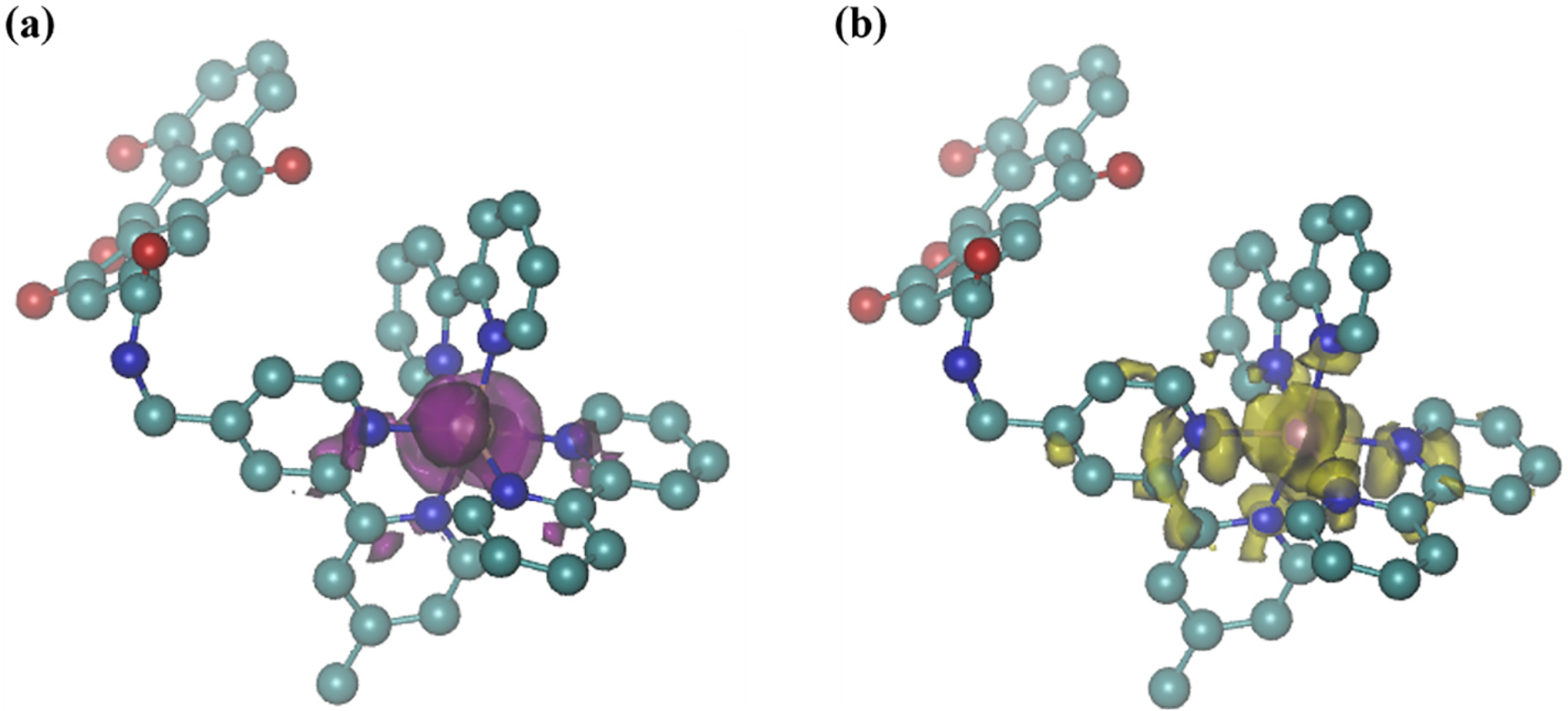

Figure 2

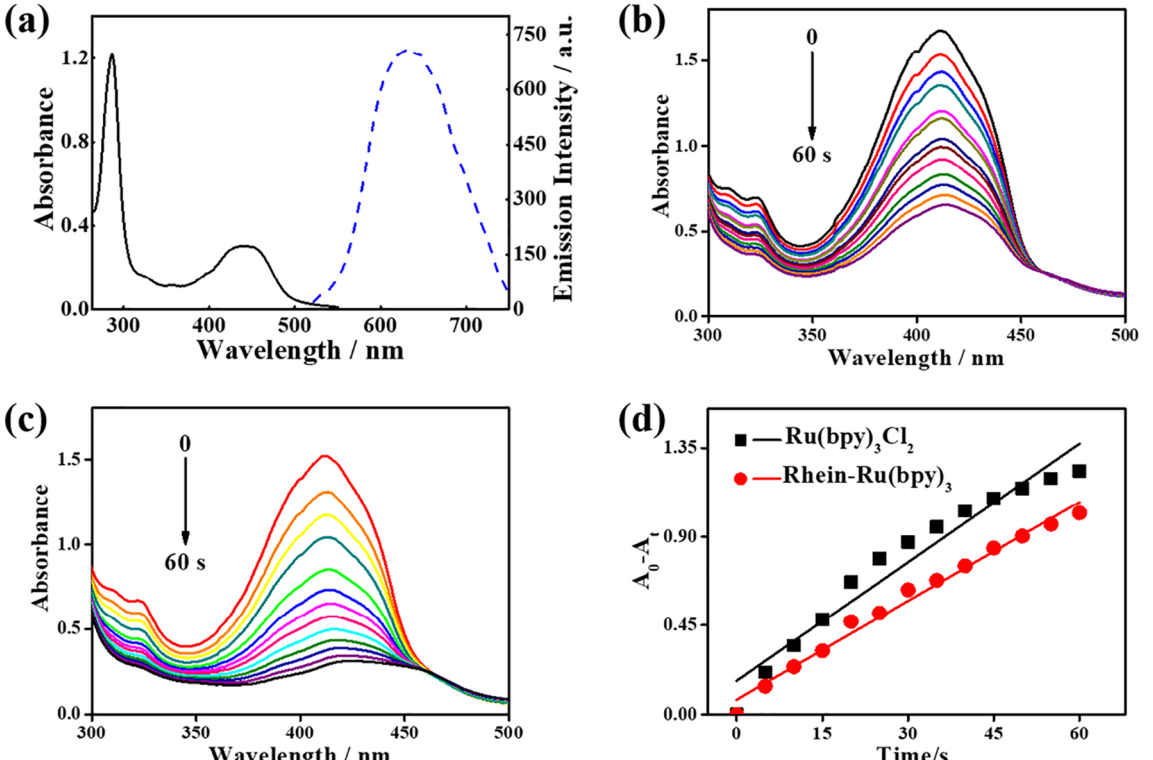
(a)
Absorbance
Emission Intensity / a.u.
Wavelength / nm
(b)
0
60 s
Absorbance
Wavelength / nm
(c)
0
60 s
Absorbance
Wavelength / nm
(d)
Ru(bpy)3Cl2
Rhein-Ru(bpy)3
A0-At
Time/s

Figure 3

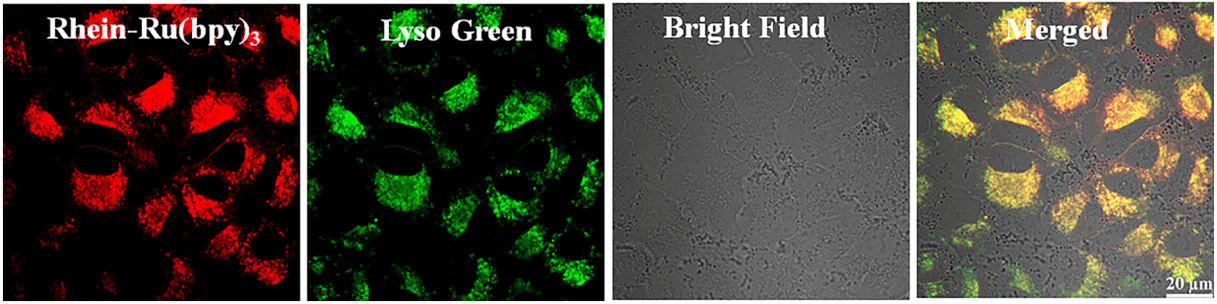

Figure 4

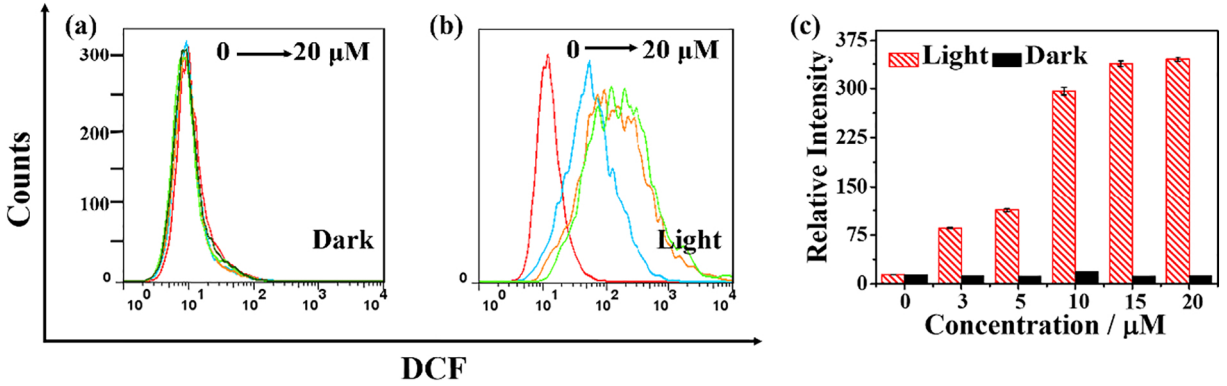
(a)
0 ⟶ 20 μM
Dark
(b)
0 ⟶ 20 μM
Light
Counts
DCF
(c)
Light
Dark
Relative Intensity
Concentration / μM

Figure 5

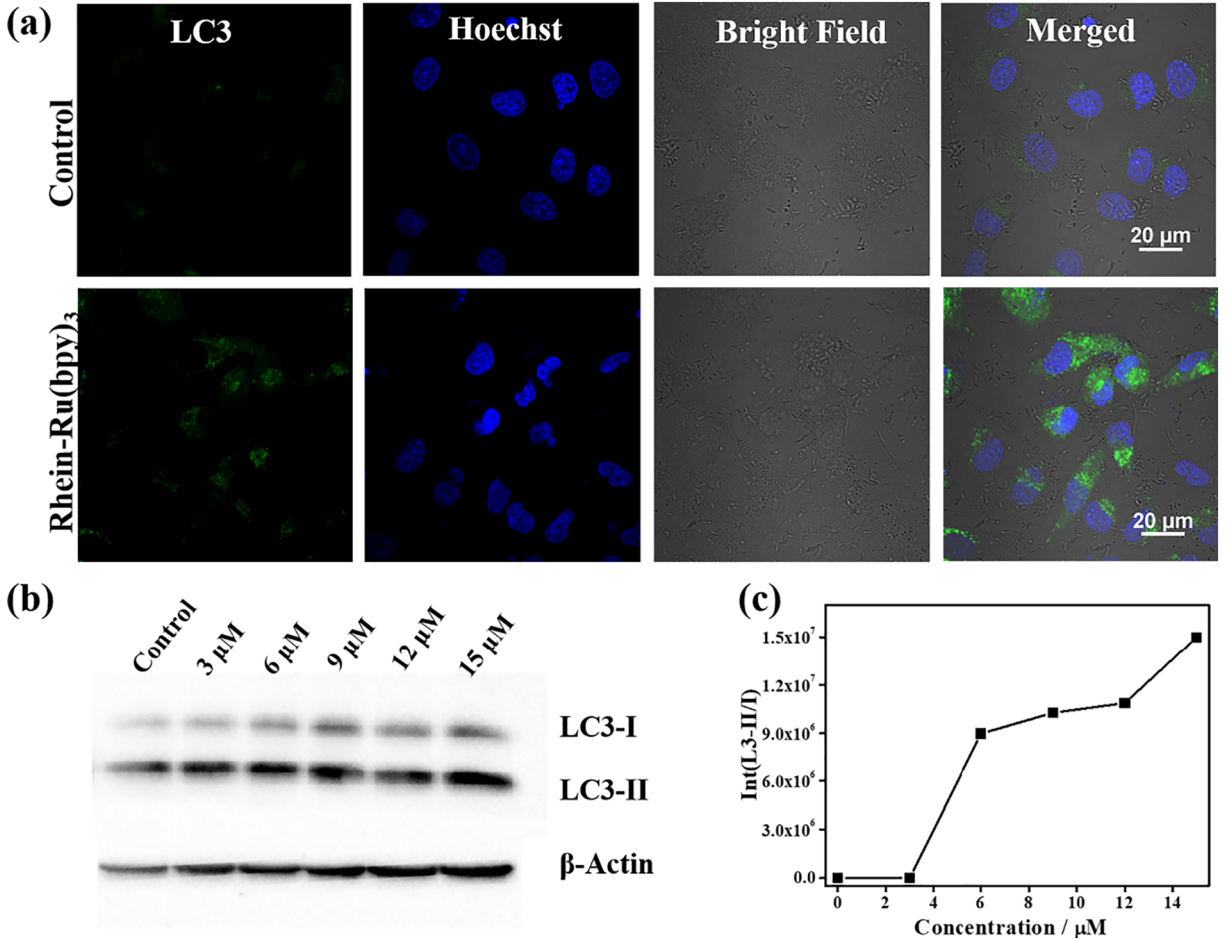
(a)
LC3
Hoechst
Bright Field
Merged
Control
Rhein-Ru(bpy)3
20 μm
20 μm
(b)
Control
3 μM
6 μM
9 μM
12 μM
15 μM
LC3-I
LC3-II
β-Actin
(c)
Int(L3-II/I)
1.5x10^7
1.2x10^7
9.0x10^6
6.0x10^6
3.0x10^6
0.0
0
2
4
6
8
10
12
14
Concentration / μM

Figure 6